Mechanism and dynamics of the reaction of XeF2 with fluorinated Si(100): Possible role of gas phase dissociation of a surface reaction product in plasmaless

Mechanism and dynamics of the reaction of XeF_2 with fluorinated Si(100): Possible role of gas phase dissociation of a surface reaction product in plasmaless etching

R. C. Hefty, J. R. Holt, M. R. Tate, and S. T. Ceyer[a)]
Department of Chemistry, Massachusetts Institute of Technology, Cambridge, Massachusetts 02139, USA

(Received 16 December 2008; accepted 24 March 2009; published online 30 April 2009)

Xenon difluoride is observed to react with Si–Si σ-dimer and σ-lattice bonds of Si(100)2×1 at 150 K by single and two atom abstraction at F coverages above 1 ML. As in the limit of zero F coverage, a measurable fraction of the scattered, gas phase product of single atom abstraction, XeF, is sufficiently internally excited to dissociate into F and Xe atoms before detection. Using the XeF internal energy and orientation distributions determined in the limit of zero coverage, the laws of conservation of momentum, energy, and mass are applied to the measured F velocity and angular distributions at higher coverage to simulate the Xe atom velocity and angular distributions and their intensities at higher coverage. The simulation predicts the observed Xe atom velocity and angular distributions at high coverage reasonably well, largely because the exothermicity channeled to XeF remains approximately constant as the coverage increases. This constancy is an opportune consequence of the trade-off between the attractiveness of the potential energy surface as the coverage is increased and the dynamics of the XeF product along the potential surface. The energy, momentum, and mass conservation analysis is also used to distinguish between Xe atoms that arise from XeF gas phase dissociation and Xe atoms that are produced by two atom abstraction. This distinction enables the calculation of percentages of the single and two atom abstraction pathways, as well as the percentages of the two pathways available to the Xe atom produced by two atom abstraction, inelastic scattering, and desorption. Finally, the simulation reveals that between 9% and 12% of F atoms produced by gas phase dissociation of XeF are scattered back toward the surface. These F atoms likely react readily with Si to form the higher fluorides that ultimately lead to etching. Gas phase dissociation of the scattered product of a surface reaction is a novel mechanism to explain the unique reactivity of XeF_2 to etch Si in the absence of a plasma. © *2009 American Institute of Physics*. [DOI: 10.1063/1.3118629]

I. INTRODUCTION

Xenon difluoride is one of the few molecules that isotropically dry etches Si in the absence of activation by a plasma.[1] This capability is critical to the integration of conventional electronics with mechanical components in a technology known as microelectromechanical systems.[2–4] The semiconductor industry's interest is not limited to Si etching. For instance, fluorine termination of dangling bonds proximate to the gate oxide has been implicated in device reliability.[5] Hence, a nonplasma method of producing reactive fluorine is broadly sought.

Consequently, there have been numerous studies and simulations of the interactions of XeF_2 and kinetics of the etching reaction of XeF_2 with Si under conditions of very high F coverage,[6–34] However, there has been little work on the mechanism and dynamics of the interaction and hence, no understanding of the origin of the very high reactivity of XeF_2 with Si. This work presents in detail the dynamics of the first steps of the etching reaction of XeF_2 on Si(100)2×1 at 150 K for F coverages up to 1.25 ML and proposes a new mechanism to explain the unique capability of XeF_2 to etch Si in the absence of a plasma.

The mechanism for reaction in the limit of zero F coverage was previously established to occur by atom abstraction,[35–37] with the possibility of both single and double F atom abstraction.[38,39] The reaction was found to proceed only at the dangling bonds of Si dimers.[40] The present work explores the effect of F coverage on the F atom single and double abstraction mechanism and specifically explores whether the abstraction mechanism remains operable at sites other than the dangling bond sites. It is known that when the dangling bonds are filled at about 1 ML of F coverage (specifically 0.9 ± 0.1 ML F), XeF_2 reacts with the σ bonds between the two Si surface dimer atoms (called σ-dimer bonds) and with the σ bonds between the surface Si atom and the Si atom one layer below (called σ-lattice bonds) with about equal probability.[40] However, it is not obvious that the mechanism remains atom abstraction, because the change in reaction site comes with a substantial change in the thermochemistry of the reaction. At zero coverage on doubly unoccupied Si–Si dangling bond sites, the reaction exothermicity for single atom abstraction is calculated to be equal to 67 kcal/mol using a theoretical value (134 kcal/mol)

[a)]Electronic mail: stceyer@mit.edu.

for the F–Si bond energy,[41] a measured value (7 kcal/mol) of the Si–Si π dimer bond energy[42,43] and the F–XeF bond energy of 60.4 ± 0.5 kcal/mol.[44] In between 0 and 1 ML F coverage, dangling bonds of singly unoccupied Si dimers are available as reaction sites. At these sites, on which the 7 kcal/mol π bond between the dangling bonds on the two Si dimer atoms no longer exists, the reaction exothermicity is calculated to be 69 kcal/mol, 2 kcal higher than on doubly unoccupied Si–Si dangling bond sites at zero coverage, using a theoretical value of 129 kcal/mol for the F–Si bond energy when each dangling bond of a Si dimer is bound to a F atom.[41] At 1 ML F coverage, the exothermicity for single atom abstraction plummets to about 15 kcal/mol for reaction at the σ-dimer and σ-lattice bonds, using a value of 54 kcal/mol for the Si–Si bond energy in crystalline Si.[45] The total energy available to the single atom abstraction products is defined as the sum of the exothermicity of the first atom abstraction event and the incident energy of the XeF_2 reactant, which is 2 kcal/mol as discussed previously[39] and below. Therefore, the total energy available to the products of a single atom abstraction at zero coverage, intermediate coverages and coverages over 1 ML are 69, 71, and 17 kcal/mol, respectively, in this experiment.

The present work also investigates the effect of higher F coverage on the gas phase dissociation of the product of the single F atom abstraction event, XeF. In the limit of zero coverage, it was shown that the product of the single atom abstraction event, XeF, is sufficiently excited by the partitioning of the available energy to its rovibrational levels to dissociate in the gas phase, less than 10^{-13} s after it was formed and within 2 Å of the surface. Specifically, the laws of conservation of momentum, energy, and mass were applied to the measured F velocity and angular distributions to simulate the Xe atom velocity and angular distributions and their intensities. The model result was found to accurately predict the observed Xe atom velocity and angular distributions.[38,39] Clearly, the potential energy surface that dictates the abstraction reaction in the limit of zero coverage is modified at higher coverage by the change in reaction exothermicity and by lateral interactions with the surrounding F atoms. In turn, the probability of XeF dissociation is governed by the amount of exothermicity channeled to XeF internal energy above its dissociation limit and by the XeF orientation in the transition state of the abstraction reaction. These effects are explored by suitably applying the zero coverage results of the energy partitioning to XeF and its orientation dependence, as determined by the conservation of momentum, energy, and mass model, to simulations of and comparison to data measured at high coverage. As at zero coverage, the energy, momentum, and mass conservation model and accompanying simulation are also used to determine the percentages of single to double atom abstraction pathways and the percentages of the two pathways available to the Xe atom produced by two atom abstraction, inelastic scattering, and desorption.

Finally, while the majority of F atoms produced by dissociation of the rovibrationally excited XeF are scattered away from the surface, the simulation shows that a small fraction of F atoms are scattered toward the surface. Atomic F is known to rapidly etch Si.[27,46] The possible role of these F atoms in producing the SiF_4 etch product observed around 1 ML coverage is discussed.

This paper is organized as follows. After a brief discussion of the experimental arrangement in Sec. II, Sec. III presents the measurements of the velocity and angular distributions of the unreacted scattered molecule XeF_2 and the XeF product. It also analyzes these data for evidence of atom abstraction at high coverage and discusses the dynamics of XeF production. Section IV presents the velocity and angular distribution measurements of scattered F and Xe, briefly reviews the energy, momentum and mass conservation model at zero coverage and then applies the model to the F and Xe atom data measured at high F coverage. Section V describes the use of the model to extract the single and two atom abstraction probabilities. Section VI discusses the possible role of gas phase dissociation of the scattered product of a surface reaction as a novel mechanism to explain the unique reactivity of XeF_2 to etch Si in the absence of a plasma.

II. EXPERIMENTAL PROCEDURE

A doubly differentially pumped molecular beam of neat XeF_2 (99+% pure, Lancaster) is incident at $\theta_i = 20°$ from the normal angle of a Si(100)(2×1) crystal held at 150 K. The stagnation pressure behind the nozzle orifice is maintained at the XeF_2 vapor pressure at 298 K. The resulting quasieffusive beam has a measured average kinetic energy of 1.4 ± 0.1 $(\pm 2\sigma)$ kcal/mol and an average internal energy of 0.6 kcal/mol, assuming a Boltzmann distribution in the rotational degrees of freedom at 298 K. A Teflon® nozzle and gas handling manifold is used to preclude contamination of the beam with free Xe produced by the decomposition of XeF_2. The amount of Xe in the beam is no larger than 0.5%.[47]

Time-of-flight (TOF) data are collected at scattering angles of $\theta_d = 15°$, 30°, and 60° from the normal angle in the forward scattering direction at each of four masses, $m/e = 167$, 148, 19, and 129, corresponding to XeF_2^+, XeF^+, F^+, and Xe^+. The flight-time distribution for each scattered product is measured by a cross-correlation TOF method described previously.[39,48] For measurements at $m/e = 167$, 148, and 19, the electron energy of the electron impact ionizer is set to 75 eV. For $m/e = 129$, it is set to 26.5 eV in order to minimize contributions from dissociative ionization of XeF_2 and XeF.

A Si crystal, determined to be clean by Auger electron spectroscopy (1% detection sensitivity limit) and ordered by He diffraction, is exposed for 34.95 s to the XeF_2 beam. During that time, TOF data are collected continuously, but are stored in eight separate but sequential bins, where a single bin is 4.38 s long. At the end of the 34.95 s exposure, the Si crystal is heated resistively at a rate of 4 K/s to above 1100 K to remove the adsorbed fluorine. This cycle of exposure and heating is repeated until a satisfactory signal-to-noise ratio is attained in the TOF spectrum. Given the incident XeF_2 flux of 0.066 ± 0.004 ML F atom/s, the data collected in bins one through eight correspond to measurements made over coverage ranges of 0–0.22, 0.22–0.40, 0.40–0.57, 0.57–0.73, 0.73–0.88, 0.88–1.01, 1.01–1.14, and

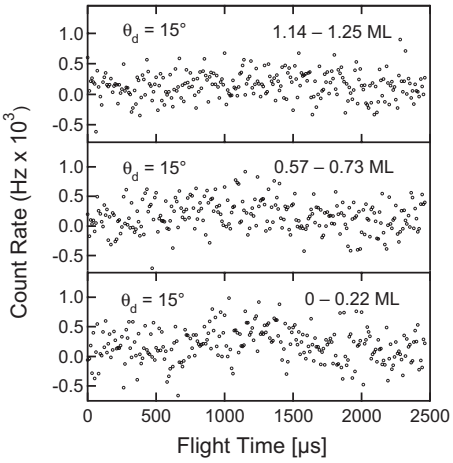

FIG. 1. XeF_2^+ TOF at $m/e=167$ measured at $\theta_d=15°$ for three coverage ranges.

1.14–1.25 ML F atoms, respectively. The exposure time is calibrated to absolute coverage by comparing the SiF_4 and SiF_2 signals measured in a thermal desorption experiment to those resulting from a known fluorine coverage, 0.94 ± 0.11 ML F atoms, as described previously.[40,49]

III. ATOM ABSTRACTION IN THE ABSENCE OF DANGLING BONDS

A. Experimental results

1. Scattered time-of-flight at m/e=167 XeF_2^+

TOF spectra recorded at $m/e=167$ result exclusively from XeF_2 that is unreactively scattered. Figure 1 shows spectra collected at $\theta_d=15°$ and for coverage ranges, 0–0.22, 0.57–0.73, and 1.14–1.25 ML F. The data are the result of signal averaging 40, 34.95 s exposures of the Si crystal to the reactant XeF_2 beam for each of the three coverage ranges shown. As evident from Fig. 1, a very small amount, less than 3%–4% of the incident XeF_2, is unreactively scattered. Spectra collected over the other five coverage ranges at $\theta_d=15°$ and over the eight coverage ranges of the two other scattering angles, 30° and 60°, exhibit similar low signal levels. Because of the low signal and apparent similarity of the spectra, the TOF spectra collected at all coverage ranges and scattering angles were averaged after being weighted by the number of spectra measured at a particular angle and coverage. The resulting average spectrum is shown in Fig. 2. The error bars represent the propagated statistical uncertainty. A Maxwell–Boltzmann distribution,[39] shown as a solid line in Fig. 2, is fit to this spectrum by varying the temperature, flow velocity, baseline count rate and scaling factor. The temperature is determined to be 194 ± 60 K resulting in an average energy and velocity of 1.49 ± 0.07 kcal/mol and 263 ± 6 m/s, respectively. The temperature, flow velocity, and background count rate so determined are then used to generate the Maxwell–Boltzmann distribution fits to the TOF spectra at each of the eight coverage ranges and at each of the three scattering angles. The best fit to the measured spectrum at each angle and coverage range is accomplished by varying the scaling factor.

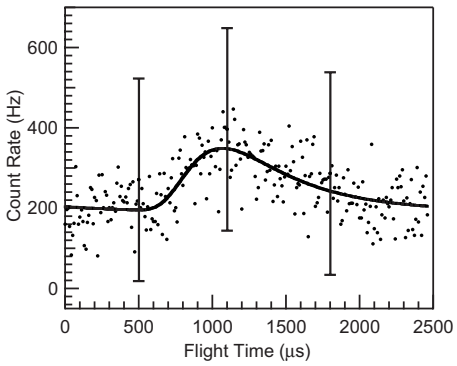

FIG. 2. XeF_2^+ TOF spectrum resulting from averaging over the TOF spectra measured at three scattering angles and eight coverage ranges at each scattering angle. Line represents fit to a Maxwell–Boltzmann distribution with $T=194\pm60$ K and average energy $=1.49\pm0.07$ kcal/mol. Error bars represent the propagated statistical uncertainty.

2. Scattered time-of-flight at m/e=148 (XeF^+)

TOF measurements at $m/e=148$ are plotted for eight coverage ranges at a scattering angle of $\theta_d=15°$ in Fig. 3. The spectra are the result of signal averaging 40 discrete exposures of the Si to the XeF_2 beam for 34.95 s. The measured spectra contain contributions not only from the XeF parent species but also from the dissociative ionization of unreactively scattered XeF_2 upon electron bombardment ionization in the mass spectrometer to form XeF^+. This contribution has been subtracted from the spectra shown in Fig. 3 as described previously.[39,50] Each spectrum is fit to a Maxwell–Boltzmann distribution shown as a line and the

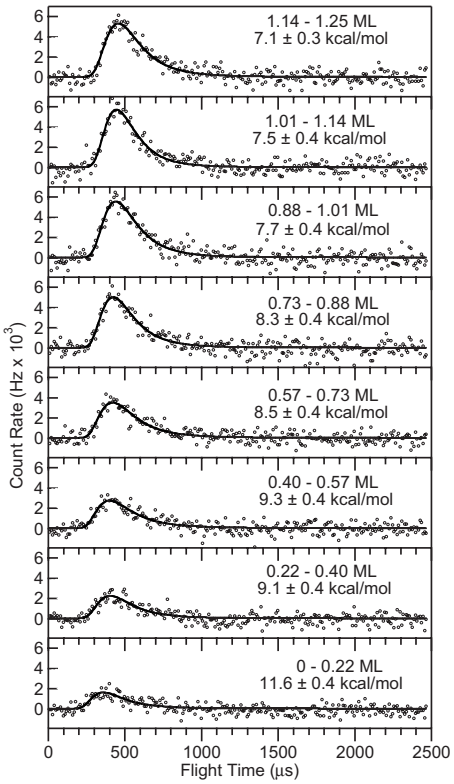

FIG. 3. Net XeF TOF spectra at $\theta_d=15°$ and eight coverage ranges. A best fit Maxwell–Boltzmann distribution function determined for each spectrum is represented by a line. Average energy of its $\pm2\sigma$ uncertainty is shown. $E_i=1.4$ kcal/mol.

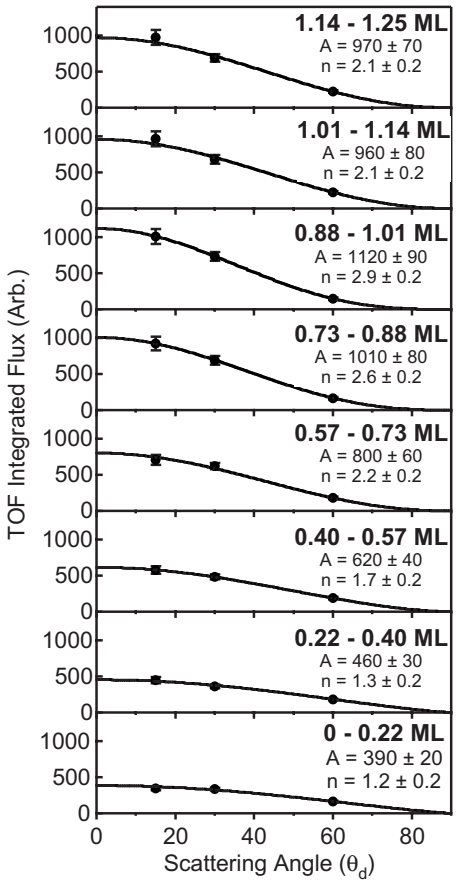

FIG. 4. Angular distribution of the XeF flux as a function of coverage. Flux determined by time integration of the velocity-weighted counts of the TOF spectrum at each scattering angle and coverage range. The error bars (slightly larger than the plotted points) represent the propagated statistical uncertainty. Line represents fit to a cosine power function (see text) with parameters shown.

average energy resulting from the fit is displayed. Similar TOF spectra[50,51] were measured over all coverage ranges at $\theta_d=30°$ and 60°, but are not shown here. For all scattering angles and coverages, the XeF translational energies are substantially greater than the XeF_2 incident energy and the energy that the XeF molecules would have had (0.60 kcal/mol) if they had desorbed in thermal equilibrium from the surface at 150 K.

The angular distributions of the scattered XeF flux for the eight coverage ranges are shown in Fig. 4. The flux at each angle, $F(\theta_d)$, is determined by time integration of the velocity-weighted counts of each TOF spectrum. The error bars represent the propagated statistical uncertainty. Each angular distribution is fit to a cosine function, $F(\theta_d)=A\cos^n\theta_d$. The best fit values for A and n are displayed with the fits shown as solid lines. Note that the angular distribution in the limit of zero coverage is almost cosine but that it becomes increasingly more peaked at the normal angle as the coverage is increased.

TOF spectra of scattered XeF were previously measured using higher XeF_2 incident energies, 1.8 and 6.3 kcal/mol, and a higher surface temperature, 250 K, as a function of coverage.[52] The average energies of these previous measurements, along with those of the present measurements are shown in Fig. 5.

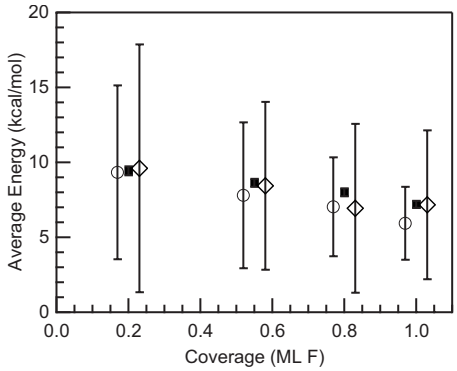

FIG. 5. Average energy of scattered XeF as a function of coverage for varying average incident energies, E_i, incident angles, scattering angles, and Si temperatures, T_{Si}. Points measured at 250 K are offset by ±0.03 ML for clarity. (○) E_i=6.3 kcal/mol, θ_i=35°, θ_d=30°, T_{Si}=250 K; (●) E_i=1.4 kcal/mol, θ_i=20°, θ_d=30°, T_{Si}=150 K; (◇) E_i=1.8 kcal/mol, θ_i=0°, θ_d=35°, T_{Si}=250 K. Large error bars on the measurements at T_{Si}=250 K are the result of a small number of experiments.

B. Discussion

The operability of the F atom abstraction mechanism at F coverages ranging from zero to 1.25 ML is clear from the observation of the scattered XeF product in the TOF spectra shown in Fig. 3 and angular distributions shown in Fig. 4. The relatively high translational energies of scattered XeF, 7.1–11.6 kcal/mol, that depend on F coverage and the dependence of the translational energy on scattering angle[52] (not shown here) indicate that the XeF product does not adsorb to the surface, equilibrate with it and then desorb. Rather, the XeF translational energy and its angular distribution are determined solely by the dynamics of the atom abstraction reaction. This conclusion is consistent with additional measurements, shown in Fig. 5, of the translational energies of XeF detected at approximately $\theta_d=30°$ and produced upon the abstraction reaction of XeF_2 incident at $\theta_i=30°$ with an energy of 6.3 kcal/mol on Si(100) at 250 K and upon reaction of XeF_2 incident at $\theta_i=0°$ with an energy of 1.8 kcal/mol on Si(100) at 250 K. It is clear from Fig. 5 that translational energies are not affected by incident energy, incident angle or surface temperature. The independence of the scattered XeF angular and energy distributions on incident conditions is consistent with the presence of strong chemical forces at the surface that eliminate memory of the initial state of XeF_2.

As determined previously, the dangling bond on each Si atom in the dimer on the Si(100)2×1 surface is the site for both abstraction and adsorption up to 1 ML of coverage. This conclusion derives from the observation by He atom diffraction that the F overlayer at 1 ML (more precisely, 0.9±0.1 ML) after exposure to XeF_2 is ordered.[40] Specifically, the size of the 2×1 unit cell of the F atom overlayer at 1 ML coverage is identical to that of the clean surface and identical to that after exposure to sufficient F_2 to produce a 1 ML overlayer. Thus, the XeF complementary fragments observed in the TOF spectra in Fig. 3 and angular distributions in Fig. 4 for coverages up to 1 ML are the products of the abstraction reaction at the dangling bond sites.

For coverages greater than 1 ML produced by continued

exposure to XeF_2, previous He atom diffraction measurements showed that the surface rapidly becomes disordered.[40] At these coverages, XeF_2 is reacting with Si–Si σ-dimer bonds and Si–Si σ-lattice bonds with equal probability. While F atom abstraction with the Si–Si bonds is less thermodynamically favorable than reaction with the dangling bonds, the abstraction reaction is still exothermic by 15 kcal/mol. Note that the exothermicity for the reaction at 1 ML is calculated assuming the Si–Si bond energy of crystalline Si.[45] It is likely that the bond energy between two Si atoms that are bonded to F atoms is lower than 54 kcal/mol, as it in Si_2F_6 compared to Si_2H_6.[53] Thus, the exothermicity of the reaction is likely higher than 15 kcal/mol, but would remain substantially below the 67 kcal/mol or 69 kcal/mol exothermicity at zero or low coverage, respectively, where the reaction occurs only at dangling bonds.

Of interest is the constancy of the available energy partitioned to translation of the XeF product as a function of coverage. As the coverage range increases from 0.73–0.88 ML to 1.14–1.25 ML, the average translational energy of XeF decreases by only 1.2 kcal/mol, from 8.3 to 7.1 kcal/mol, even though the available energy decreases from 71 kcal/mol to 17 kcal/mol as the abstraction reaction site moves from dangling bonds to Si–Si σ-bonds. The constancy of the XeF translational energy is a consequence of the trade-off between the attractiveness of the potential energy surface, which is determined by the reaction exothermicity in a barrierless reaction, and the percentage of energy partitioned to product translation, or equivalently, the dynamics of XeF as it moves along the potential energy surface. The less attractive the potential energy surface becomes, the higher the percentage of the exothermicity transferred to translation as opposed to the vibration of the newly formed SiF bond.[54] For example, on a very exothermic potential surface, such as at low coverage, the reactant picks up speed as it progresses through the entrance channel. By the time the reactant reaches the bend leading to the exit channel, it is moving so fast that it misses the turn, and instead, climbs up on the potential energy surface shoulder where the repulsion between the two atoms that ultimately will form the new bond is very high. This repulsion, in turn, sets up a motion known as the bobsled effect that effectively converts the available energy into vibration of the newly formed bond instead of into translation of the scattered XeF product.[54] So, at the lower F coverages of 0.73–0.88 ML, where the available energy is higher (71 kcal/mol), a smaller percentage of the available energy, 12%, is partitioned to translation than at higher coverages where the available energy is lower but where the percentage of available energy partitioned to translation is higher, about 30%. Hence, the absolute value of the energy partitioned to translation is about constant.

It should be noted that this general relationship between the dynamics of the reaction product and the shape of the potential energy surface is strictly valid only for collinear collisions. It is unlikely that the atom abstraction reaction is collinear at low coverage because the XeF angular distributions in Fig. 4 are described by a cosine function, indicative of either a floppy transition state that results in scattering of the product over a wide angular range or a wide range of angles of approach of the reactant to the dangling bonds that result in reaction. In contrast, at higher coverages, the XeF angular distribution narrows, becoming more sharply peaked at the surface normal. The presence of Si–F groups may provide sufficient steric hindrance to limit the angles of the XeF_2 approach for a successful reaction with the Si–Si bonds to those approaches with collinear geometry. The presence of Si–F groups may also channel the outgoing trajectory of XeF in a more normal direction to the surface. This narrowing of the potential energy surface at higher F coverage and the consequent change in the dynamics of the reactants and products may also play a role in counteracting the decrease in the attractiveness of the potential surface, resulting in partitioning of a larger amount of the available energy into translation than the decrease in the attractiveness of the potential surface alone would predict.

IV. GAS PHASE DISSOCIATION OF A PRODUCT OF A SURFACE REACTION

A. Experimental results

1. Scattered time-of-flight at $m/e=19$ (F^+)

TOF spectra of the scattered F atoms are plotted in Fig. 6 for eight coverage ranges and three scattering angles. The spectra at $\theta_d=15°$ and 60° are signal averaged over 40, 34.95 s exposures of Si to XeF_2 and the spectrum at $\theta_d=30°$ is signal averaged over 81 exposures. The contribution to this spectrum from F^+ arising from dissociative ionization of XeF_2 in the ionizer has been subtracted as described previously.[39,50] The contribution due to dissociative ionization of XeF to form F^+ has also been removed from this spectrum by multiplying the Maxwell–Boltzmann fit to the corresponding XeF spectrum by the fragmentation ratio, $\sigma_{XeF\rightarrow F^+}/\sigma_{XeF\rightarrow XeF^+}$, where $\sigma_{XeF\rightarrow F^+}$ and $\sigma_{XeF\rightarrow XeF^+}$ are the cross sections for dissociative ionization and ionization of the species shown, respectively, and then subtracting this result point by point from the $m/e=19$ spectrum. The fragmentation ratio is determined by finding its maximum value that does not produce a negative F atom count rate upon subtraction from the measured $m/e=19$ signal in any of the 24 TOF spectra (one spectrum for each of the eight coverage ranges at each of three scattering angles). This value is determined to be 0.4 and is set by the $m/e=19$ TOF spectrum measured at a scattering angle of 15° and a coverage range of 0.88–1.25 ML F. Comparison of the F atom TOF spectra in Fig. 6 to the XeF_2 spectrum in Fig. 1 or Fig. 2 or the XeF spectra in Fig. 3 reveals that the spectra are very different. The maximum of the F atom spectrum appears at shorter times than that of the XeF_2 or XeF spectra. This difference shows unambiguously that F atoms do not arise from dissociative ionization of XeF_2 or XeF in the detector.

2. Scattered time-of-flight at $m/e=129$ (Xe^+)

TOF spectra of the scattered Xe atoms are plotted in Fig. 7 for eight coverage ranges and three scattering angles. The spectra at $\theta_d=30°$ and 60° are signal averaged over 160, 34.95 s exposures of Si to XeF_2 and the spectrum at $\theta_d=15°$ is signal averaged over 80 exposures. The contribu-

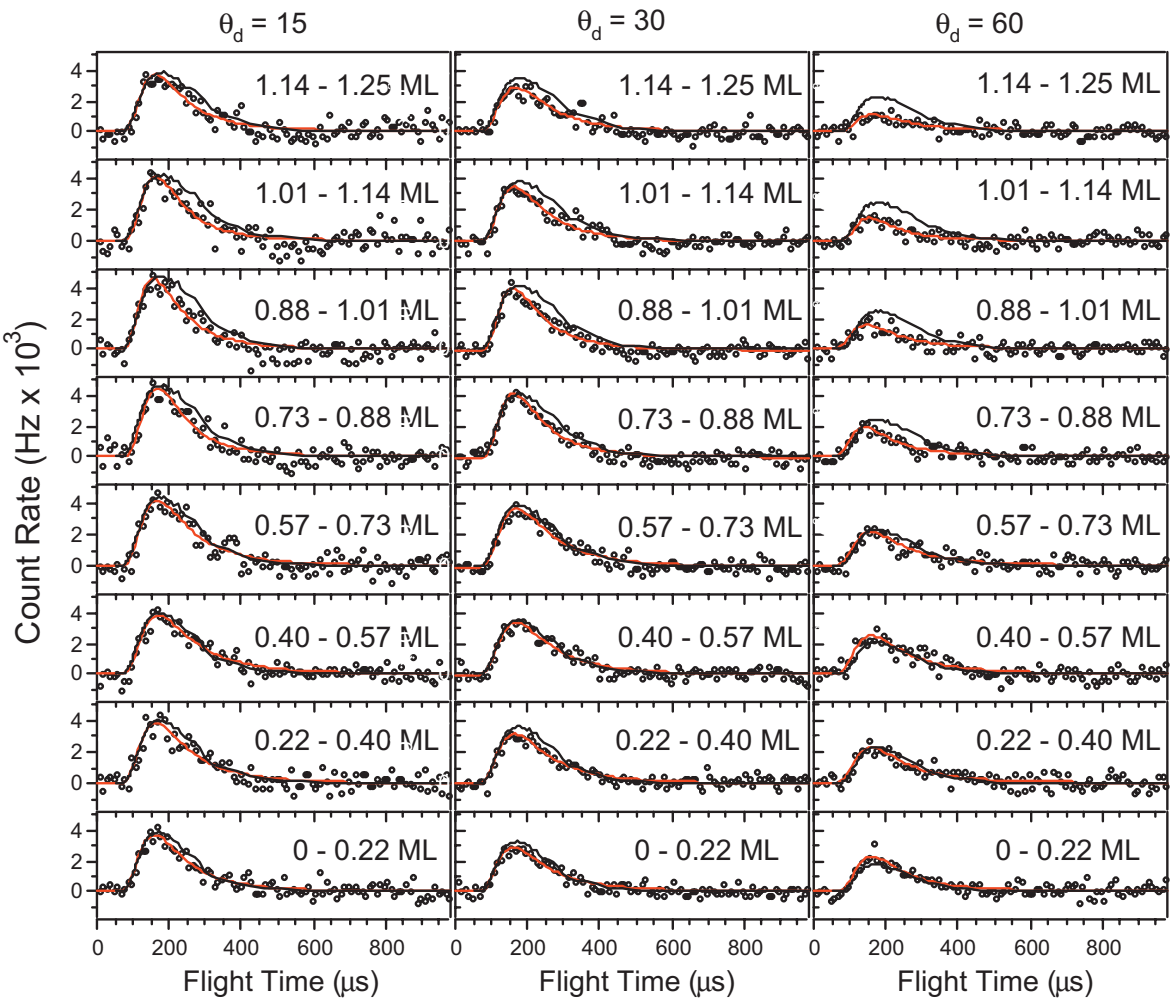

FIG. 6. (Color) Net F atom TOF spectra at three scattering angles and eight coverage ranges. A best fit Maxwell–Boltzmann distribution function determined for each spectrum is represented by a red line (Ref. 39). Black line is simulated result.

tion to this spectrum from Xe^+ arising from dissociative ionization of XeF_2 has been subtracted as described previously.[39,50] The contribution due to dissociative ionization of XeF to form Xe^+ has also been removed from this spectrum by multiplying the Maxwell–Boltzmann fit to the corresponding XeF spectrum by the fragmentation ratio, $\sigma_{XeF\rightarrow Xe^+}/\sigma_{XeF\rightarrow XeF^+}$, where $\sigma_{XeF\rightarrow Xe^+}$ and $\sigma_{XeF\rightarrow XeF^+}$ are the cross sections for dissociative ionization and ionization of the species shown, respectively, and then subtracting this result point by point from the $m/e=129$ spectrum. The value of this fragmentation ratio is 0.5. Use of a larger value yields Xe fluxes at coverages greater than 0.57 ML that are substantially lower than the simulated results for the Xe flux.[39,50] The simulated Xe atom flux has been described previously[39,50] and is summarized below.

B. Gas phase dissociation of XeF in the limit of zero coverage: Summary of model

As demonstrated previously in the limit of zero coverage, the observed F atoms are produced by dissociation of the XeF product in the gas phase, when the XeF molecules are approximately 2 Å from the surface.[38,39] Dissociation results when at least 3 kcal, the XeF bond dissociation energy, of the 69 kcal/mol energy available to the abstraction reaction is channeled into rovibrational excitation of the scattered XeF molecule. The internal energy above the dissociation energy is converted to translational energy of the F and Xe atoms moving away from each other in opposite directions in the center of mass frame.

A model was developed to unambiguously demonstrate that the observed F atoms arise from the gas phase dissociation of XeF.[39,50,51] The model predicts the Xe atom velocity and angular distributions and their intensities by applying the laws of conservation of momentum, energy, and mass to the measured F velocity and angular distributions. The measured XeF velocity and angular distributions are used to convert to laboratory coordinates. It is found that the predictions for the Xe distributions agree with the measured Xe velocity and angular distributions to within the experimental uncertainties. A summary of the model is given here.

The conservation of momentum and energy relationships in the center of mass frame are defined by Eqs. (1) and (2), respectively,

$$m_{Xe}\vec{v}_{Xe}^{cm} = -m_F\vec{v}_F^{cm}, \quad (1)$$

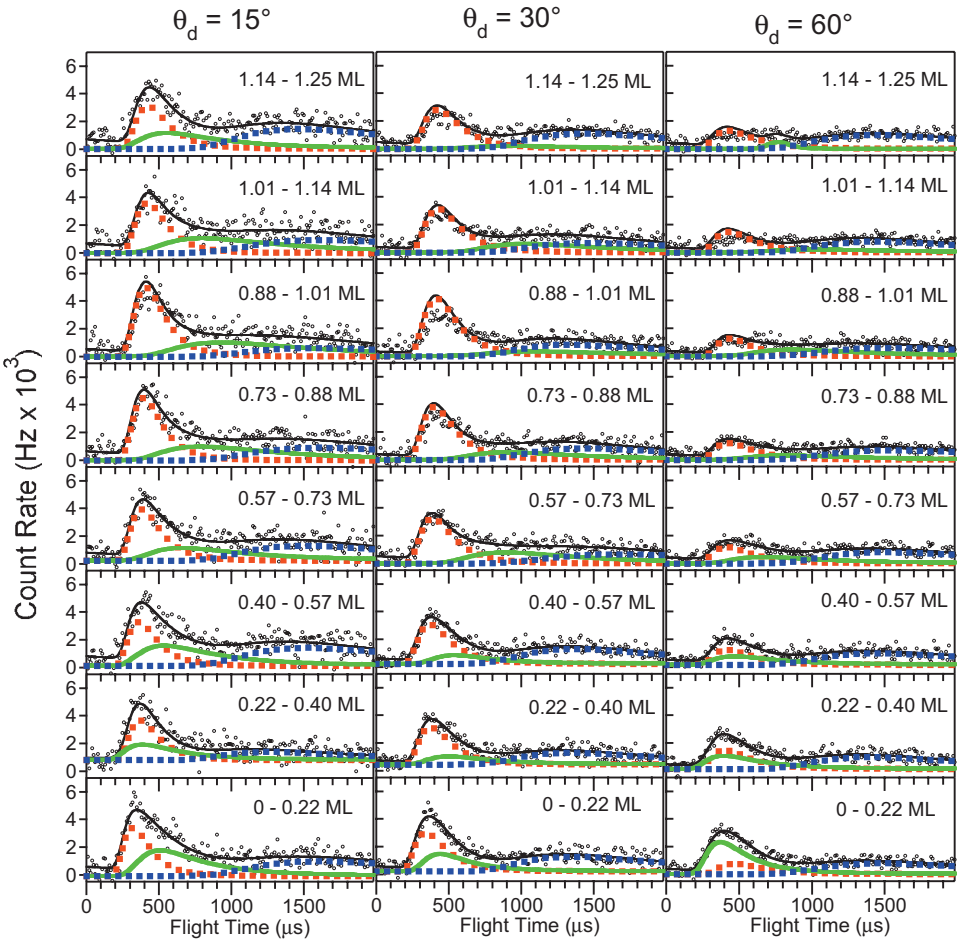

FIG. 7. (Color) Net Xe atom TOF spectra for three scattering angles and eight coverage ranges. Red dashed line represents simulated Xe spectra. Green solid line and blue dashed line represent inelastically scattered and thermally accommodated Xe atoms, respectively, from two atom abstraction. Black solid line represents sum of simulated spectrum, inelastically scattered and thermally accommodated Xe atom contributions. Uncertainty in the simulation is 22% of the simulated intensity, arising largely from the 20% uncertainty in the F atom ionization cross section.

$$\tfrac{1}{2}m_{\mathrm{Xe}}|\vec{v}_{\mathrm{Xe}}^{\mathrm{cm}}|^2+\tfrac{1}{2}m_{\mathrm{F}}|\vec{v}_{\mathrm{F}}^{\mathrm{cm}}|^2=E_{\mathrm{int}}(\mathrm{XeF})-E_{\mathrm{diss}}(\mathrm{XeF})=E_{\mathrm{cm}}, \tag{2}$$

where m is the mass and $\vec{v}^{\mathrm{cm}}$ is the center of mass velocity of the designated species. Equation (2) sets the sum of F and Xe atom translational energies after dissociation equal to the difference between the available reaction energy partitioned to the XeF internal degrees of freedom, $E_{\mathrm{int}}(\mathrm{XeF})$, and the XeF bond dissociation energy, $E_{\mathrm{diss}}(\mathrm{XeF})$. This difference is defined as E_{cm}, which is the XeF internal energy that is converted to translational energy of the Xe and F atoms upon XeF dissociation. Solving Eqs. (1) and (2) for the center of mass velocities yields

$$|\vec{v}_{\mathrm{F}}^{\mathrm{cm}}|=\sqrt{\frac{2E_{\mathrm{cm}}}{m_{\mathrm{F}}\left(1+\frac{m_{\mathrm{F}}}{m_{\mathrm{Xe}}}\right)}}\quad |\vec{v}_{\mathrm{Xe}}^{\mathrm{cm}}|=\sqrt{\frac{2E_{\mathrm{cm}}}{m_{\mathrm{Xe}}\left(1+\frac{m_{\mathrm{Xe}}}{m_{\mathrm{F}}}\right)}}. \tag{3}$$

Because $\vec{v}_{\mathrm{F}}^{\mathrm{cm}}$ is determined from the F atom TOF spectra measured in the laboratory frame, E_{cm} can be calculated from the first equality in Eq. (3). In turn, E_{cm} is used in the second equality in Eq. (3) to predict $\vec{v}_{\mathrm{Xe}}^{\mathrm{cm}}$ and those predictions are ultimately compared to the measured Xe atom TOF spectra. Before either $\vec{v}_{\mathrm{F}}^{\mathrm{cm}}$ can be determined or a comparison of $\vec{v}_{\mathrm{Xe}}^{\mathrm{cm}}$ to the measured Xe atom velocities can be made, these center of mass velocities must be converted to laboratory frame vectors. The Newton diagram in Fig. 8 illustrates this conversion and defines θ as the scattering angle of XeF with respect to the surface plane and ϕ as the XeF bond axis orientation with respect to $\vec{v}_{\mathrm{XeF}}$. Both θ and ϕ are essential quantities in the coordinate conversion.[39] Because the measured F laboratory velocities and scattering angles are distributions of velocities and angles, E_{cm} and $\theta+\phi$ are also distributions, denoted as $I(E_{\mathrm{cm}})$ and $I(\theta+\phi)$, respectively.

Using Eq. (4), the simulated velocity and angular distributions, $I^{\mathrm{lab}}_{\mathrm{F\ or\ Xe}}(v^{\mathrm{lab}}_{\mathrm{F\ or\ Xe}},\chi_{\mathrm{F\ or\ Xe}})$, where $\chi_{\mathrm{F\ or\ Xe}}=90°-\theta_d$, are determined by summing of a large number of calculated trajectories:

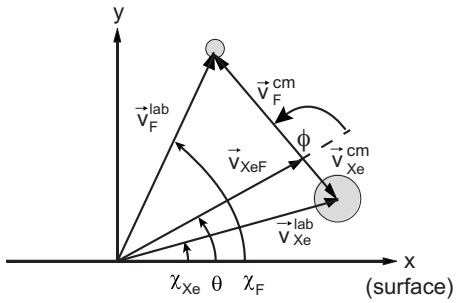

FIG. 8. Newton diagram relating center of mass and laboratory frame velocity vectors for gas phase dissociation of XeF. Note that $\chi_{\mathrm{F}}=90°-\theta_d$ and $\chi_{\mathrm{Xe}}=90°-\theta_d$.

$$I^{\mathrm{lab}}_{\mathrm{F\ or\ Xe}}(v^{\mathrm{lab}}_{\mathrm{F\ or\ Xe}}(v_{\mathrm{XeF}}),\chi_{\mathrm{F\ or\ Xe}}(\theta)) = \left(\frac{v^{\mathrm{lab}}_{\mathrm{F\ or\ Xe}}}{v^{\mathrm{cm}}_{\mathrm{F\ or\ Xe}}}\right)^2 I(\theta+\phi)P(\theta,v_{\mathrm{XeF}})P(v^{\mathrm{cm}}_{\mathrm{F\ or\ Xe}}), \quad (4)$$

where $P(\theta,v_{\mathrm{XeF}})$ is the measured XeF velocity flux distribution at a laboratory scattering angle θ, and $P(v^{\mathrm{cm}}_{\mathrm{F\ or\ Xe}})$ is the F or Xe atom center of mass velocity probability distribution calculated from $I(E_{\mathrm{cm}})$. Each trajectory has a set of initial conditions given by $\{\phi,\theta,v_{\mathrm{XeF}},E_{\mathrm{cm}}\}$. Specifically, 25 discrete values are used for θ, 33 values for ϕ, 70 values for v_{XeF}, and 140 values for E_{cm}. Thus, the resulting simulation matrix contains 8 085 000 trajectories for each measured F (or Xe) atom TOF spectra. Each element in this matrix represents a single F (or Xe) atom trajectory resulting from a specific set of XeF initial conditions.

The functions $I(E_{\mathrm{cm}})$ and $I(\theta+\phi)$ are optimized to fit simultaneously the three measured F atom TOF distributions in the coverage range of 0–0.22 ML in Fig. 6, as described in detail previously.[39] The functional form of $I(E_{\mathrm{cm}})$ with its single parameter E_{cm} that yields the best fit is $I(E_{\mathrm{cm}})=(RT)^{-1}\exp(-E_{\mathrm{cm}}/RT)$ with an average center of mass energy $\bar{E}_{\mathrm{cm}}=3.9\pm0.7$ kcal/mol where $T=1970$ K. The average amount of available energy channeled into the XeF internal degrees of freedom is thus $\bar{E}_{\mathrm{int}}=8.4$ kcal/mol. The functional form of $I(\theta+\phi)$ with its single parameter ϕ that yields the best fit of the simulated F atom distributions to the measured TOF and angular distributions of scattered F atoms is

$$I(\theta+\phi)=1 \quad \text{for} \quad -30^\circ \le \theta+\phi < 210^\circ \quad \text{and}$$
$$I(\theta+\phi)=0 \quad \text{for} \quad -30^\circ > \theta+\phi \ge 210^\circ. \quad (5)$$

Physically, this range of molecular orientations means that initial conditions with the XeF bond axis within $\pm120°$ from the normal and with the F end of the XeF molecule pointing away from the surface are included in the simulation, and conditions with the F end pointing toward the surface and within $\pm60°$ of the normal are not. As discussed below, the XeF bond axis orientations with the F end pointing toward the surface and within $\pm60°$ of the normal are those that contribute to two atom abstraction.

Simulated spectra using the best fit functions for $I(E_{\mathrm{cm}})$ and $I(\theta+\phi)$ are plotted as black lines in Fig. 6 for the coverage range of 0–0.22 ML along with the measured spectra (dots) and the accompanying fit of the spectra to a Maxwell–Boltzmann distribution (red lines). The intensities of the simulated spectra are obtained by multiplying each point of each spectrum by the same normalization constant. The constant is determined by normalizing the intensity of the maximum value of the simulated spectrum at $\theta_d=15°$ to 1.05 times the intensity of the corresponding point of the measured spectrum at $\theta_d=15°$.[39]

Once $I(E_{\mathrm{cm}})$ and $I(\theta+\phi)$ are optimized to accurately reproduce the F atom TOF and angular distributions, they are used to predict $I^{\mathrm{lab}}_{\mathrm{Xe}}(v^{\mathrm{lab}}_{\mathrm{Xe}},\chi_{\mathrm{Xe}})$ using Eq. (4). To introduce conservation of mass, the simulated Xe atom spectral intensities are normalized such that the total number of Xe atoms integrated over all scattering angles is equivalent to the total number of F atoms in the simulated F atom spectra integrated over all scattering angles. The normalized simulated Xe atom velocity distribution is then transformed into a number density distribution in time and compared, as a red dashed line in Fig. 7, with the experimental spectra in the 0–0.22 ML coverage range. The agreement between simulated and experimental spectra is excellent. At $\theta_d=15°$ and 30°, where the contribution of Xe atoms from gas phase dissociation is the greatest and hence, where the comparison of the model and data is most sensitive, the simulation accurately predicts the rapid rise and flux of fast Xe atoms at short flight times. The quantitative agreement between experimental and simulated TOF spectra for the fastest Xe atoms is the basis for the previous conclusion that XeF dissociates in the gas phase unperturbed by the surface.[38,39]

The simulation does not account for the entire Xe atom TOF distributions at $\theta_d=15°$ and 30°, nor the TOF spectrum at $\theta_d=60°$ because two other channels for Xe atom production not associated with gas phase dissociation are present. They are discussed in Sec. V.

C. Gas phase dissociation of XeF at high F coverages

The zero coverage limit was initially chosen as the coverage over which to determine $I(E_{\mathrm{cm}})$ and $I(\theta+\phi)$, because reaction sites are most homogeneous and hence, the exothermicity of the reaction is most uniform. In addition, because the coverage is low, the number of reactive events that occur nearby a Si site occupied by a F atom is minimal, thus minimizing the effect of variation of the interaction potential and maximizing the homogeneity of $I(E_{\mathrm{cm}})$ and $I(\theta+\phi)$.

This section explores the extension of the XeF gas phase dissociation model to the abstraction reaction at higher coverages, using the optimal functions for $I(E_{\mathrm{cm}})$ and $I(\theta+\phi)$ that were determined for the coverage range, 0–0.22 ML F. Specifically, these functional forms are used in Eq. (4) to simulate the F atom spectra for each of the seven higher coverage ranges, from 0.22 ML up to 1.25 ML. The XeF angle-resolved TOF spectra measured at each of the seven higher coverage ranges at which the simulation is carried out are used to convert from center of mass to laboratory coordinates. The intensities of the simulated spectra are obtained by multiplying each point of each spectrum by the same normalization constant used for all three spectra at 0–0.22 ML.

The simulated F atom spectra at the higher coverage ranges are shown in Fig. 6. While the simulated spectra at the 0.22–0.40, 0.40–0.57, and 0.57–0.73 ML range of coverages do not fit the measured spectra as well as the simulated spectra for the 0–0.22 ML coverage range, the agreement is within the statistical error of the data for all nine simulated spectra. For the coverage ranges of 0.73–0.88, 0.88–1.01, 1.01–1.14, and 1.14–1.25 ML, the simulated spectra lie slightly outside of the statistical uncertainty of the measured TOF spectra. In particular, the simulations at higher coverage predict a larger flux of slow F atoms than is observed, a feature discussed below.

Using the best fit functions $I(E_{\mathrm{cm}})$ and $I(\theta+\phi)$ at 0–0.22 ML, the Xe atom spectra are predicted at the seven higher

coverage ranges. The angle-resolved XeF TOF spectrum at each coverage range is employed to convert from the center of mass to the laboratory coordinates. As in the limit of zero coverage, the simulated Xe atom spectral intensity at a given coverage is normalized such that the number of Xe atoms integrated over all scattering angles is equivalent to the angle-integrated number of F atoms in the simulated F atom spectra at a given coverage. The normalized Xe atom simulated spectra are plotted as red dashed lines along with the experimental spectra for all coverage ranges in Fig. 7. The agreement between the simulated and experimental spectra is very good for each of the scattering angles at higher coverages. In particular, the simulation accurately predicts the rapid rise and flux of fast Xe atoms at short flight times and predicts the flight times of the Xe atoms at flight times at which they are observed. The simulated spectra at the shortest flight times lie within the statistical error of the data and the simulated intensity for all coverage ranges and scattering angles.

As noted above, simulations at higher coverage predict a slightly higher flux of slow F atoms than observed but describe the fast portion of the spectrum well. An increase in the value of $\bar{E}_{cm}$ in the function $I(E_{cm})$ would yield faster F atoms, but such a change shifts the entire simulated F atom velocity distribution to higher values, rather than removing flux from the slower end of the distribution. A more promising remedy is narrowing the angular range of the function $I(\theta+\phi)$, so that there are fewer orientations with the F end of the XeF molecule pointing toward the surface that contribute to dissociation. This modification shifts flux of slow F atoms to higher velocities, while having little effect on the velocities of the Xe atoms, because the Xe velocities are so low compared to the F atom velocities. A narrower range of molecular XeF bond orientations at higher coverages is physically plausible because the increased steric repulsion between the unreactive F end of XeF_2 and the adsorbed F atoms hinders the approach of the reacting F end of XeF_2 to the dangling bonds or Si–Si σ-bonds. Nevertheless, the functions determined in the limit of low coverage work remarkably well to describe the dynamics of XeF dissociation at high coverage. In particular, the applicability of the same function $I(E_{cm})$ to the XeF dissociation dynamics at higher coverages implies that the partitioning of the available energy to the internal degrees of freedom is unchanged from the value in the limit of zero coverage, $\bar{E}_{int}=8.4$ kcal/mol, and is consistent with the small change in partitioning of translational energy to XeF with coverage discussed in Sec. III B.

Also consistent with the almost constant energy partitioning with coverage is the observation that the percentage of XeF dissociation does not vary substantially with coverage. The analysis, presented in more detail in Sec. V, shows that $79\pm3\%$ of the XeF product formed by single atom abstraction dissociates in the limit of zero coverage while $72\pm3\%$ dissociates at 1.25 ML coverage.

V. TWO ATOM ABSTRACTION AND RELATIVE REACTION PROBABILITIES

A. Two pathways for two atom abstraction

The Xe atoms observed in Fig. 7 that are not accounted for by the simulated TOF spectra resulting from the gas phase dissociation of XeF arise from two atom abstraction. Two atom abstraction refers to reaction of the XeF product with the Si surface via an additional F atom abstraction reaction, resulting in adsorption of both F atoms of the XeF_2 reactant and production of a gas phase Xe atom. This pathway occurs when XeF does not escape the attractive interaction with the surface.

As discussed previously,[39] the XeF product molecules that undergo atom abstraction are those whose bond axis orientations have the F atom end pointed toward the surface. Molecules so oriented experience a larger attractive interaction with the Si surface. The attractive interaction pulls XeF into the surface whereupon the F atom is abstracted, leaving the Xe atom to collide with the surface and eventually back scatter. This interaction is the origin of the omission of XeF trajectories with the F end of the XeF molecule pointing toward the surface and with a bond axis orientation within $\pm60°$ of the normal in the simulation. However, as discussed above, the simulation predicts a slightly higher flux of slow F atoms than observed at higher coverage, implying that XeF orientations greater than $\pm60°$ from the normal (with the F end of the XeF molecule pointing toward the surface) could reasonably be omitted in the simulation at higher coverage.

During or after the abstraction event, the Xe atom collides with the surface. The Xe atom may lose sufficient energy to the surface to be trapped. If so, the Xe atom equilibrates with the surface and eventually desorbs with an average energy equal to $2kT$, where T is the surface temperature of 150 K, characteristic of a Maxwell–Boltzmann energy distribution. The intensity of the thermally accommodated distribution is fitted as described previously[39] and is plotted as a blue dashed line in Fig. 7. As is apparent, the Maxwell–Boltzmann distribution describes well the low energies of Xe atoms for all coverages, demonstrating that some Xe atoms are indeed desorbing from the surface.

However, the Xe atom may not lose sufficient energy to be trapped when it collides with the surface during or after the abstraction event. In this case, the Xe atom scatters inelastically. These Xe atoms are apparent in Fig. 7 at flight times intermediate to those Xe atoms produced by XeF dissociation and those trapped Xe atoms produced by two atom abstraction. Their distribution is represented in Fig. 7 by a green solid line and is obtained by the following procedure. The measured Xe TOF distribution is fit to the sum of three distribution functions corresponding to the three channels by which Xe is produced, XeF dissociation, thermal desorption after two atom abstraction, and inelastic scattering after two atom abstraction, and is represented by the black solid line in Fig. 7. The parameters of the simulated distribution and those of the thermal distribution at 150 K are held constant while the parameters of the Maxwell–Boltzmann distribution of inelastically scattered Xe atoms are adjusted until the sum of the three distributions fit the entire Xe atom TOF distri-

TABLE I. Percentages of thermally desorbed and inelastically scattered Xe atoms produced by two atom abstraction. Error bars represent $\pm\sigma$ statistical uncertainty.

Coverage (ML)	% Xe equilibrated	% Xe inelastic
0–0.22	33 ± 4	67 ± 4
0.22–0.40	43 ± 8	57 ± 8
0.40–0.57	53 ± 4	47 ± 4
0.57–0.73	56 ± 1	44 ± 1
0.73–0.88	61 ± 2	39 ± 2
0.88–1.01	52 ± 5	48 ± 5
1.01–1.14	76 ± 4	24 ± 4
1.14–1.25	87 ± 2	13 ± 2

bution well. The overall fit agrees with the measured data at all coverages and scattering angles to within the statistical error of the data.

The ratio of two atom abstraction events that lead to inelastically scattered Xe atoms to those that lead to thermally accommodated Xe atoms can be evaluated from the angle-integrated fluxes of each contribution to the TOF spectra using the following procedure. The inelastically scattered Xe flux, as determined by integrating the velocity-weighted distribution shown by a green solid line in Fig. 7 over time, is plotted (not shown here) for each of the three scattering angles. The resulting angular distribution is fit to a cosine power function and integrated over scattering angle to yield the total angle-integrated flux of Xe atoms that were produced by inelastic scattering. An identical procedure is used to determine the total angle-integrated flux of Xe atoms that thermally accommodate. These absolute fluxes are used to calculate the corresponding percentages shown in Table I as a function of coverage.

In the limit of zero coverage, 67% of the Xe atoms produced by two atom abstraction inelastically scatter. As the F coverage increases to about 0.5 ML, the percentage of Xe atoms that thermally accommodates becomes about equal to the percentage that inelastically scatters. The ratio remains one until 1 ML coverage where the percentage of equilibrated Xe atoms climbs to 76% and continues to climb to 87% at 1.25 ML F coverage. The increase in the probability for thermal accommodated likely arises from the increased energy transfer from Xe to the surface upon collision with the F covered surface. The F covered surface is less stiff and rougher than the clean Si lattice, leading to a larger degree of energy loss by the Xe atom and hence, a greater chance that the Xe atom becomes trapped.

As discussed previously,[39] XeF dissociation produces a small fraction (2.5%) of Xe atoms whose trajectories are aimed at the surface. These Xe atoms contribute to the measured thermally accommodated and inelastically scattered fraction but their contribution is within the statistical error of the measurements.

B. Two atom versus single atom abstraction

Three sources for Xe atom production exist: gas phase dissociation, Xe atoms from two atom abstraction that inelastically scatter, and Xe atoms from two atom abstraction that thermally equilibrate with the surface. From the above discussion, it is clear that the simulation enables resolution of the Xe TOF spectrum into the three contributions. Knowledge of the flux of each component allows probabilities for each pathway of the XeF_2 reaction with Si to be calculated.

The percentages of unreactively scattered XeF_2, of XeF scattered intact, of dissociated XeF as well as the percentages of single atom and two atom abstraction, calculated from the measured fluxes of XeF_2, XeF, and Xe, are shown in Table II. Because the masses and ionization potentials of XeF_2, XeF, and Xe are relatively similar, their transmission probabilities through the quadrupole and ionization probabilities, respectively, are considered to be equal. The angle-integrated flux of inelastically scattered and thermally accommodated Xe is determined as described in Sec. IV. The two atom abstraction percentage is calculated from the sum of the angle-integrated inelastically scattered and thermally accommodated Xe flux minus the Xe flux directed at the surface from XeF dissociation. However, because the percentage of Xe flux with trajectories aimed at the surface as a result of XeF dissociation is so small (2.5% of the dissociating XeF) as discussed previously,[39] its contribution to the two atom abstraction percentage is not removed. The angle-integrated XeF_2 and XeF fluxes are determined similarly, but the loss of flux due to dissociative ionization of the XeF_2 and XeF parent species in the electron bombardment ionizer is accounted

TABLE II. Percentages of unreactively scattered XeF_2, of XeF produced by single atom abstraction that reaches the detector intact, of XeF produced by single atom abstraction that dissociates and of Xe produced by two atom abstraction. The percentage of single atom abstraction is the sum of the percentages of intact XeF and dissociated XeF. Error bars represent $\pm\sigma$ statistical uncertainty.

Coverage (ML)	% unreacted XeF_2	% intact XeF	% dissociated XeF	% one atom abstraction	% two atom abstraction
0–0.22	4 ± 1	9 ± 1	34 ± 2	43 ± 2	53 ± 5
0.22–0.40	4 ± 1	12 ± 1	48 ± 3	60 ± 4	36 ± 7
0.40–0.57	4 ± 1	12 ± 1	38 ± 2	50 ± 2	45 ± 5
0.57–0.73	3 ± 1	13 ± 1	43 ± 1	56 ± 1	41 ± 1
0.73–0.88	3 ± 1	15 ± 1	48 ± 1	63 ± 1	33 ± 2
0.88–1.01	3 ± 1	15 ± 1	48 ± 2	63 ± 2	33 ± 2
1.01–1.14	3 ± 1	17 ± 1	48 ± 2	65 ± 2	32 ± 3
1.14–1.25	3 ± 1	17 ± 1	44 ± 2	61 ± 2	36 ± 2

for. The angle-integrated XeF_2 flux is used to calculate the percentage of unreacted XeF_2 while that of XeF is used to calculate the percentage of intact XeF. The percentage of dissociated XeF is calculated from the velocity-weighted integration of the simulated Xe flux, shown as the red dashed line in Fig. 7. The integrated simulated Xe flux is plotted as a function of scattering angle and the resulting angular distribution is fit to a cosine power function and integrated over scattering angle to yield the angle-integrated simulated Xe flux, as carried out previously.[39] This quantity is equivalent to the flux of XeF that dissociates. The percentage of single atom abstraction is the sum of the percentages of intact XeF and dissociated XeF.

The percentage of unreactively scattered XeF_2 is very small, about 3%–4% of the product flux from the reactive channels at all coverages. The small percentage is a consequence of the very high reaction probability of the XeF_2. The percentage of XeF_2 that reacts by single atom abstraction is 43% in the 0–0.22 ML range, while the percentage that reacts by two atom abstraction is 53%. The higher percentage of two atom abstraction in the limit of zero coverage is reasonable because nearly all dangling bond sites are available for reaction. The percentage reverses to 60% single atom and 36% two atom abstraction as soon as the coverage builds to 0.22–0.40 ML and remains relatively constant up to 1.25 ML. Thus, as the dangling bonds become decorated with F atoms, the abstraction probability of the second F atom decreases. The presence of adsorbed F atoms may shield the attractive interaction between XeF and the Si surface in addition to sterically hindering its approach to Si.

Because the single atom abstraction percentage increases slightly with coverage, both the percentage of XeF scattered intact and dissociated XeF increase slightly. As noted in the previous section, of the XeF produced by single atom abstraction, the percentage of XeF that dissociates does not change substantially with coverage. About $79 \pm 3\%$ of the XeF formed dissociates in the limit of zero coverage. This percentage decreases to about $72 \pm 3\%$ at 1.25 ML F. The relative constancy of the percent dissociation of XeF is consistent with the almost constant energy partitioning over the entire coverage range of 0–1.25 ML F.

VI. ROLE OF GAS PHASE DISSOCIATION IN XeF_2 ETCHING OF Si

The reaction rate of XeF_2 with Si to form volatile SiF_4 is known to be 10^3–10^4 times higher than that of F_2 (Refs. 26, 27, 31, and 34) despite the fact that the F_2 reaction is 25 kcal/mol more exothermic than the XeF_2 reaction.[40] The origin of the reactivity difference is not understood. A recent study showed that the interaction of XeF_2 with Si(100) for coverages lower than 1 ML is identical to that of F_2.[40] In both cases, the dangling bonds abstract F atoms until each dangling bond is decorated with a F atom, forming an ordered 2×1 overlayer at about 1 ML coverage. Unlike F_2, which ceases reacting with Si at 1 ML coverage, XeF_2 continues to react, ultimately depositing sufficient fluorine to form SiF_4 that then desorbs.[40,49] Figure 9 shows the SiF_4 produced (measured as SiF_3^+ because the cross section for dissociative ionization of SiF_4 to produce SiF_3^+ is much larger than the cross section for ionization of SiF_4 to produce SiF_4^+) as a function of F coverage. These measurements are carried out by directing the XeF_2 beam at the Si held at 150 K while monitoring the SiF_3^+ signal in the differentially pumped mass spectrometer as a function of exposure at several different detector angles. The known XeF_2 exposures are converted to coverage as described above. The data at $\theta_d = 15°$ show that SiF_4 production begins at a detectable level above about 1 ML of F coverage. The relative decrease in the signal at larger detector angles reflects a narrowing angular distribution peaked at the surface normal.

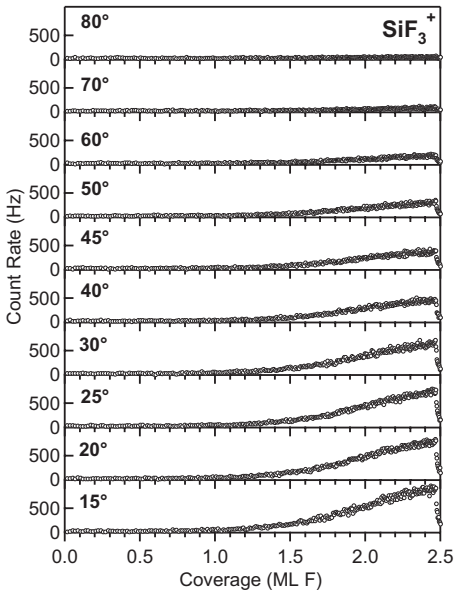

FIG. 9. Scattered SiF_4, measured as SiF_3^+ at $m/e=85$, as a function of coverage for varying scattering angles, θ_d. The signal decreases precipitously at 2.45 ML F because the XeF_2 beam is turned off.

The mechanism for SiF_4 formation from two Si surface atoms each bonded to a F atom is unknown, but it is interesting to consider the role that the F atoms directed at the surface upon XeF dissociation may play in the formation of SiF_2, SiF_3, and SiF_4. Figure 10 shows simulated angular distributions of the F atoms, described in detail previously, as a function of coverage. It is clear that the F atom flux does not go to zero at $\theta_d=90°$. Fluorine atoms scattered at angles greater than 90° are aimed toward the surface. Integration of the angular distributions over the intervals $90° \leq \theta_d \leq 180°$ and $-180° \leq \theta_d \leq -90°$ and over all values of the out of plane scattering angle yields between 9% and 12% of the total F atom flux aimed at the surface. At coverages below 1 ML, these F atoms are captured by dangling bonds, but at higher coverages where no dangling bonds are available, these F atoms react with Si–Si σ-dimer and σ-lattice bonds yielding SiF_2 and SiF_3 species that ultimately form volatile SiF_4. Indeed, F atoms are known to react with Si–Si lattice bonds and thus to etch Si efficiently.[27,46]

The velocity distributions of these F atoms are different from those F atoms scattered away from the surface because XeF velocities aimed toward the surface are not allowed in the simulation and because the XeF bond axis orientation is restricted to ±120° of the surface normal. Figure 11 shows

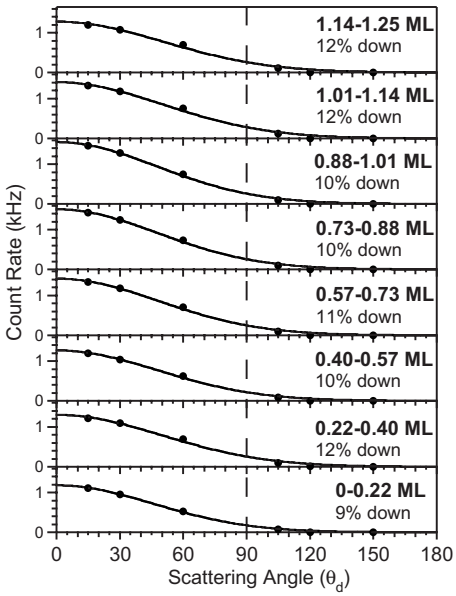

FIG. 10. Angular distributions of simulated F atom flux as a function of scattering angle for eight coverage ranges. Line is the best fit to the simulated flux values shown as dots. The percentage of F atom flux aimed at the surface is given as percentage down.

the simulated TOF of F atoms produced in the 1.14–1.25 ML coverage range for different scattering angles. At $\theta_d = 105°$ and 120°, the F atoms are faster, on the average, than at lower angles, because there are fewer combinations of XeF velocity vectors and XeF bond orientations that result in slower atoms scattered at these angles. For example, a F atom scattering angle of 120° can be achieved with the XeF bond axis making a 120° angle to the surface normal, with the F end of XeF oriented toward the surface, and the XeF velocity close to zero. Given that the velocity of XeF is close to zero for these trajectories, the observed F atom velocity is largely determined by the center of mass energy, E_{cm}. At

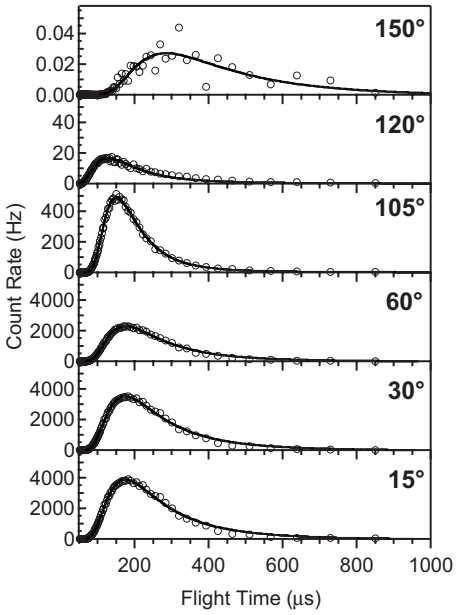

FIG. 11. Simulated F atom TOF spectra for a range of scattering angles, θ_d, at a 1.14–1.25 ML coverage range. Line represents a Maxwell–Boltzmann fit to the spectra.

150°, the F atom distribution is on the average slower than at scattering angles below 90° because fewer trajectories result in fast atoms being scattered at these angles. For example, scattering of a F atom at $\theta_d = 150°$ requires that the F end of XeF be oriented toward the surface, the XeF velocity be large and the XeF scattering angle, θ_d, be negative.

Production of these F atoms with trajectories aimed at the surface may be one reason for the extreme difference in reactivity of F_2 and XeF_2.[40] In the case of F_2, once a F atom is abstracted, the complementary F atom with a trajectory away from the surface has no chance to reverse its trajectory and head back toward the surface.[36,37] In contrast, the F atom of the complementary XeF fragment with a trajectory away from the surface does have a second chance to react if the XeF dissociates and the resulting F atom has a trajectory aimed at the surface. This incident F atom reacts with a Si–Si bond resulting not only in its adsorption but also in the production of a dangling bond that can readily abstract a F atom from an incident XeF_2 molecule. Hence, these F atoms may have a catalytic effect on the reaction rate. Gas phase dissociation of a surface reaction product likely plays the critical role in the overall chemistry of the plasmaless etchant, XeF_2. Additional investigations on this question are in progress.

VII. SUMMARY

Xenon difluoride reacts with unfluorinated Si(100) with near unit probability. About 43% of the XeF_2 reacts at dangling bond sites via single atom abstraction to produce scattered XeF. Of the XeF produced, about 79% dissociates in the gas phase to form a F atom and a Xe atom. While the majority of the F atoms scatter away from the surface, about 10% of them have trajectories aimed at the surface where they are captured by dangling bonds. The remaining 53% of the incident XeF_2 undergoes two atom abstraction to produce scattered Xe. About 67% of the Xe is inelastically scattered while 33% thermally accommodates with the Si and then desorbs.

As the F atom coverage increases to 1.25 ML, both single and two atom abstraction continue to operate as the mechanisms by which XeF_2 reacts, even though dangling bond sites are unavailable when the coverage reaches about 1 ML. As determined earlier, both the Si–Si σ-dimer bonds and σ-lattice bonds become the reaction sites at 0.9 ± 0.1 ML of F.[40] The abstraction reaction remains unactivated at these sites. The single atom abstraction pathway becomes more probable (about 63%) than two atom abstraction because of site blocking by the adsorbed F atoms and because the surface becomes less attractive for steering the XeF toward it. A higher percentage of thermally accommodated Xe atoms, 87%, is observed than at low coverage because the less stiff F overlayer allows for more inelasticity and hence a larger trapping fraction.

Gas phase dissociation of the product of the surface reaction, XeF, also remains operable and the percentage of XeF that dissociates remains approximately constant at 72% as the coverage increases. The percentage remains constant because the absolute amount of energy partitioned to XeF remains constant, even though the exothermicity of the

single atom abstraction reaction decreases by 52 kcal/mol as the coverage increases from 0 to 1.25 ML. This constancy is an opportune consequence of the trade-off between the attractiveness of the potential energy surface and the fraction of energy partitioned to the product. The less attractive the potential energy surface becomes, the higher the percentage of the exothermicity transferred to the XeF product as opposed to the vibration of the newly formed SiF bond. Thus, the conservation of energy, momentum, and mass model that was developed at zero coverage to unambiguously demonstrate that the XeF dissociated in the gas phase applies reasonably well at higher coverages.

Finally, the model and its accompanying simulation reveal that between 9% and 12% of the F atoms produced by gas phase dissociation of XeF are scattered back toward the surface. These F atoms react readily with the Si lattice to form the higher fluorides that result in SiF_4 formation and ultimately in etching of the Si. This insight is made possible only by the simulation, which has been shown to agree well with the measured angular and velocity distributions of the F atoms and Xe atoms that are scattered away from the surface. Gas phase dissociation of the scattered product of a surface reaction is a novel mechanism to explain the unique reactivity of XeF_2 to etch Si in the absence of a plasma.

ACKNOWLEDGMENTS

This work was supported by the National Science Foundation under Grant No. CHE-0517786.

[1] K. R. Williams and R. S. Muller, J. Microelectromech. Syst. **5**, 256 (1996).
[2] I. C. Ressejac, L. M. Landsberger, and J. F. Currie, J. Vac. Sci. Technol. A **18**, 746 (2000).
[3] N. H. Tea, V. Milanovic, C. A. Zincke, J. S. Suehle, M. Gaitan, M. E. Zaghloul, and J. Geist, J. Microelectromech. Syst. **6**, 363 (1997).
[4] G. T. A. Kovacs, N. I. Maluf, and K. E. Petersen, Proc. IEEE **86**, 1536 (1998).
[5] T. B. Hook, E. Adler, F. Guarin, J. Lukaitis, N. Rovedo, and K. Schruefer, IEEE Trans. Electron Devices **48**, 1346 (2001).
[6] H. F. Winters, D. B. Graves, D. Humbird, and S. Tougaard, J. Vac. Sci. Technol. A **25**, 96 (2007).
[7] E. Kobayashi, K. Isari, and K. Mase, Surf. Sci. **528**, 255 (2003).
[8] C. Herrmann, D. Chen and J. J. Boland, Phys. Rev. Lett. **89**, 096102 (2002).
[9] S. R. Qiu and J. A. Yarmoff, Phys. Rev. B **63**, 115409 (2001).
[10] D. C. Hays, K. B. Jung, Y. B. Hahn, E. S. Lambers, S. J. Pearton, J. Donahue, D. Johnson, and R. J. Shul, J. Electrochem. Soc. **146**, 3812 (1999).
[11] M. J. M. Vugts, G. L. J. Verschueren, M. F. A. Eurlings, L. J. F. Hermans, and H. C. W. Beijerinck, J. Vac. Sci. Technol. A **14**, 2766 (1996).
[12] M. J. M. Vugts, M. F. A. Eurlings, L. J. F. Hermans, and H. C. W. Beijerinck, J. Vac. Sci. Technol. A **14**, 2780 (1996).
[13] M. L. Yu and L. A. DeLouise, Surf. Sci. Rep. **19**, 285 (1994).
[14] M. J. M. Vugts, G. J. P. Joosten, A. van Oosterum, H. A. J. Senhorst, and H. C. W. Beijerinck, J. Vac. Sci. Technol. A **12**, 2999 (1994).
[15] C. W. Lo, P. R. Varekamp, D. K. Shuh, T. D. Durbin, V. Chakarian, and J. A. Yarmoff, Surf. Sci. **292**, 171 (1993).
[16] C. W. Lo, D. K. Shuh, V. Chakarian, T. D. Durbin, P. R. Varekamp and J. A. Yarmoff, Phys. Rev. B **47**, 15648 (1993).
[17] H. F. Winters and J. W. Coburn, Surf. Sci. Rep. **14**, 162 (1992).
[18] V. M. Bermudez, J. Vac. Sci. Technol. A **10**, 3478 (1992).
[19] R. A. Haring and M. Liehr, J. Vac. Sci. Technol. A **10**, 802 (1992).
[20] F. A. Houle, J. Chem. Phys. **87**, 1866 (1987).
[21] J. A. Dagata, D. W. Squire, C. S. Dulcey, D. S. Y. Hsu, and M. C. Lin, J. Vac. Sci. Technol. B **5**, 1495 (1987).
[22] B. Roop, S. Joyce, J. C. Schultz, and J. I. Steinfeld, Surf. Sci. **173**, 455 (1986).
[23] F. R. McFeely, J. F. Morar, and F. J. Himpsel, Surf. Sci. **165**, 277 (1986).
[24] B. Roop, S. Joyce, J. C. Schultz, N. D. Shinn, and J. I. Steinfeld, Appl. Phys. Lett. **46**, 1187 (1985).
[25] B. Roop, S. Joyce, J. C. Schultz, and J. Steinfeld, J. Chem. Phys. **83**, 6012 (1985).
[26] D. E. Ibbotson, J. A. Mucha, and D. L. Flamm, J. Appl. Phys. **56**, 2939 (1984).
[27] D. E. Ibbotson, D. L. Flamm, J. A. Mucha, and V. M. Donnelly, Appl. Phys. Lett. **44**, 1129 (1984).
[28] J. F. Morar, F. R. McFeely, N. D. Shinn, G. Landgren, and F. J. Himpsel, Appl. Phys. Lett. **45**, 174 (1984).
[29] N. D. Shinn, J. F. Morar, and F. R. McFeely, J. Vac. Sci. Technol. A **2**, 1593 (1984).
[30] F. R. McFeely, J. F. Morar, N. D. Shinn, G. Landgren, and F. J. Himpsel, Phys. Rev. B **30**, 764 (1984).
[31] M. J. Vasile, J. Appl. Phys. **54**, 6697 (1983).
[32] H. F. Winters and F. A. Houle, J. Appl. Phys. **54**, 1218 (1983).
[33] T. J. Chuang, J. Appl. Phys. **51**, 2614 (1980).
[34] H. F. Winters and J. W. Coburn, Appl. Phys. Lett. **34**, 70 (1979).
[35] Y. L. Li, D. P. Pullman, J. J. Yang, A. A. Tsekouras, D. B. Gosalvez, K. B. Laughlin, M. T. Schulberg, D. J. Gladstone, M. McGonigal, and S. T. Ceyer, Phys. Rev. Lett. **74**, 2603 (1995).
[36] M. R. Tate, D. Gosalvez-Blanco, D. P. Pullman, A. A. Tsekouras, Y. L. Li, J. J. Yang, K. B. Laughlin, S. C. Eckman, M. F. Bertino, and S. T. Ceyer, J. Chem. Phys. **111**, 3679 (1999).
[37] M. R. Tate, D. P. Pullman, Y. L. Li, D. Gosalvez-Blanco, A. A. Tsekouras, and S. T. Ceyer, J. Chem. Phys. **112**, 5190 (2000).
[38] R. C. Hefty, J. R. Holt, M. R. Tate, D. B. Gosalvez, M. F. Bertino, and S. T. Ceyer, Phys. Rev. Lett. **92**, 188302 (2004).
[39] R. C. Hefty, J. R. Holt, M. R. Tate, and S. T. Ceyer, J. Chem. Phys. **129**, 214701 (2008).
[40] J. R. Holt, R. C. Hefty, M. R. Tate, and S. T. Ceyer, J. Phys. Chem. B **106**, 8399 (2002).
[41] S. P. Walch, Surf. Sci. **496**, 271 (2002).
[42] M. P. D'Evelyn, Y. L. Yang, and L. F. Sutcu, J. Chem. Phys. **96**, 852 (1992).
[43] U. Hofer, L. Li, and T. F. Heinz, Phys. Rev. B **45**, 9485 (1992).
[44] P. C. Tellinghuisen, J. Tellinghuisen, J. A. Coxon, J. E. Velazco, and D. W. Setser, J. Chem. Phys. **68**, 5187 (1978).
[45] R. Walsh, Acc. Chem. Res. **14**, 246 (1981).
[46] C. D. Stinespring and A. Freedman, Appl. Phys. Lett. **48**, 718 (1986).
[47] B. Itin, A. Bielecki, R. C. Hefty, J. R. Holt, R. G. Griffin, and S. T. Ceyer (unpublished).
[48] S. T. Ceyer, D. J. Gladstone, M. McGonigal, and M. T. Schulberg, *Physical Methods of Chemistry*, edited by B. W. Rossiter and R. C. Baetzold, 2nd ed. (Wiley, New York, 1993), Vol. IXA, p. 383.
[49] D. P. Pullman, A. A. Tsekouras, Y. L. Li, J. J. Yang, M. R. Tate, D. B. Gosalvez, K. B. Laughlin, M. T. Schulberg, and S. T. Ceyer, J. Phys. Chem. B **105**, 486 (2001).
[50] R. C. Hefty, Ph.D. thesis, Massachusetts Institute of Technology, 2004.
[51] J. R. Holt, Ph.D. thesis, Massachusetts Institute of Technology, 2002.
[52] M. R. Tate, Ph.D. thesis, Massachusetts Institute of Technology, 1999.
[53] H. Koinuma, T. Manako, and K. Fueki, Jpn. J. Appl. Phys., Part 2 **25**, L471 (1986).
[54] R. D. Levine and R. B. Bernstein, *Molecular Reaction Dynamics and Chemical Reactivity* (Oxford University Press, New York, 1987).